A lowenergy approach to process large scale airflow

A low-energy approach to process large scale airflow

Yimin SHAO[1], Yang BAI[1], Yongjia WU[2], Tingzhen MING[2], Renaud de RICHTER[3], Xianfeng FAN[1] , Xiaohua LU[4], Wei LI[1]*

[1] Institute for Materials and Processes, School of Engineering, The University of Edinburgh, Edinburgh EH9 3FB, Scotland, UK

[2] School of Civil Engineering and Architecture, Wuhan University of Technology No.122 Luoshi Road, Hongshan District, Wuhan 430070, China

[3] Tour-Solaire.fr, 8 Impasse des Papillons, Montpellier 34090, France

[4] College of Chemical Engineering, State Key Laboratory of Materials-oriented Chemical Engineering, Nanjing Tech University, Nanjing 211816, China

**Corresponding author, Wei.Li@ed.ac.uk*

Graphical Abstract:

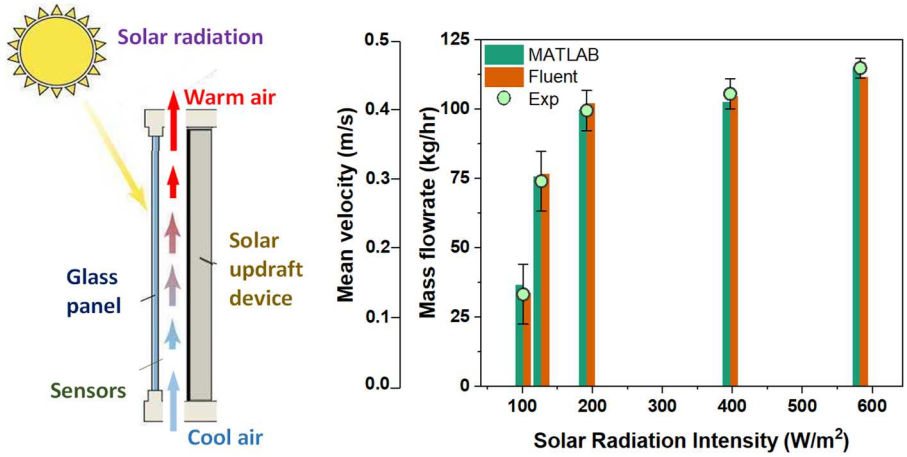

Novelty statement:

- A simplified solar updraft device designed and built to process large scale airflow.
- Low intensity solar radiation, e.g. 120 W/m^2, is enough to generate considerable updraft.
- Two numerical models developed to assist design and application of solar updraft devices.

Abstract:

A simplified solar updraft device adapted from the Trombe wall concept was built to process large scale airflow using only solar energy. The performances were systematically studied using experimental measurements and numerical models, with the focus of investigating whether this device can generate enough airflow under low solar intensities, and developing a fast-analytical mathematical model to effectively and efficiently find design rules for further application. The experimental results prove that the air mass flowrate generated by solar updraft in a 0.9 m^2 solar updraft device can be as

high as 75.6 kg/hr when the solar radiation is only 120 W/m^2. Comparison of two numerical models shows that it is feasible to develop a fast-analytical tool based on widely available MATLAB with low demand of computing resources and to provide guidance on how a future device should be designed for particular applications. The study also investigated the effects of a wider range of solar radiation intensities, air channel height and thickness on the updraft performances (e.g. air temperature, airflow velocity and mass flow rate).

Keywords: Greenhouse Gas Removal, Direct air capture, Solar Energy, updraft, CFD simulation

1. Introduction

A wide portfolio of negative emission technologies (NET) is needed to achieve net zero. A low-energy and versatile approach which can remove multiple greenhouse gases (GHGs) (e.g. CO_2, CH_4, N_2O, etc.) simultaneously from the air can be a game changer.

The first step for such an ideal technology is to develop an air processing unit at a large scale but with low energy demand. Because 1) Greenhouse Gas Removal (GGR) from the air at a large scale requires sufficient airflow given the extreme dilution of the greenhouse gases, 2) it is energy-intensive to generate sufficient airflow (e.g. the energy required to generate airflow in a Direct Air Capture process can account for 20 - 30% (i.e. 60 - 90 KJ/molCO_2) of the entire energy consumption) [1, 2].

Recently, de Richter et.al. proposed to utilize solar energy to create an updraft, facilitate CO_2 capture and drive photocatalytic decomposition of CH_4 and N_2O [3-5]. The proposed technology has been discussed and endorsed as an emerging technology for GGR in three independent reports from the Intergovernmental Panel on Climate Change [6, 7] and the Royal Society [8].

A series of feasibility studies are needed to advance the above-untested concept into a transformative technology. The first question is – can the technology be deployed around the globe? i.e. can moderately low solar radiation (e.g. in most European countries) generate sufficient updraft?

There are several solar updraft designs investigated in recent years. Trombe wall is one of the most adaptable formats and it has advantages including low cost of building materials, small footprint, simple structure, and high thermal efficiency [9, 10]. The current focus is the performance of C-shaped flow channel in Trombe wall to improve thermal efficiency and air quality of a built environment.

The updraft airflow rate was investigated by several research groups using numerical methods. For example, Gan investigated the influence of Trombe wall parameters on space heating through CFD simulation [11]. Lal et al. studied the potential of a modified solar chimney for space heating [12]. The result shows that under 500 W/m^2 solar intensity, different air cavity thickness (from 0.06 to 0.14 m) produced different airflow rates (from 5.18 to 18.14 kg/hr), while the height and width of the wall were 3.1 m and 0.3 m, respectively. Wu et al. studied the performance of the multi-functional Trombe wall. Their results show that the airflow it can generate varied with the channel height and width under different solar radiation intensity. When solar intensity was 200 W/m^2, the airflow rate was approximately in the range of 9.44 to 18.88 kg/hr in different designs [13]. The same research group also reported that an optimized Trombe wall (with 1 m height, 1 m width, 0.05 m air cavity thickness) could generate 31.8 to 53.1 kg/hr airflow under varied solar radiation intensity, based on data obtained via numerical method [14]. Du et al. also applied modelling to demonstrate that changing the geometry of the wall can affect air velocity [15].

There are more comprehensive study based on both experimental and numerical methods. Yu et al. showed that a Trombe wall (1 m height, 0.5 m width, 0.09 m air cavity thickness) could produce airflow rate in the range of 16.2 to 56.7 kg/hr under 300 to 800 W/m^2 solar intensity [16-19]. Mokni et al. conducted an experimental study in Saudi Arabia under actual climatic circumstances to investigate the influence of climatic factors (including solar intensity) on Trombe wall. Their results show that the airflow increased from 127 to 339.84 kg/hr when solar intensity raised from 100 to 800 W/m^2 [20].

There are also some researchers focusing on designing modified Trombe wall to improve its heating performance, using more intricate structures or combining with other components. Ahmed et al. investigated the effects of a porous medium, a fan, and a glass cover on the performance of a PV/Trombe wall. The findings showed adding the porous medium and fan had positive effects on the system performance and an empirical formula for air velocity and solar radiation intensity was established. Under 130 W/m^2 solar intensity, a modified C-shape Trombe wall (height 2 m width 0.68 m and thickness0.1 m) can produce 45.062 kg/hr [21]. Some other intricate structures or additions are also demonstrated, e.g. addition of fins[22], selective absorbing coating [23] and venetian blind structure [24], and wavy-shaped wall etc [25].

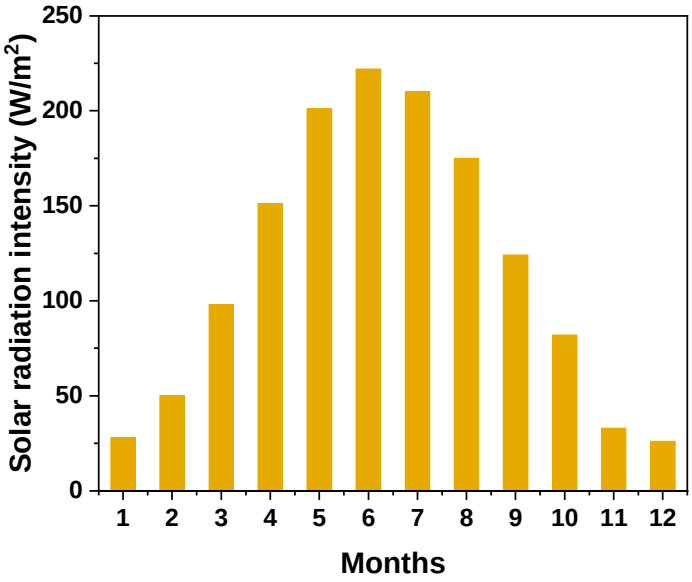

Fig.1 Monthly average solar radiation in south England [26].

From the above studies, we found that 1) There are scarce experimental data of airflow rate on real conditions (e.g. under low solar radiation typically in the Europe as show in Fig 1). 2) Different dimensions of a Trombe wall has a great impact on the updraft capacity under both high and low solar intensities. 3) A simpler and more general model is needed for more insights that are necessary for efficient design and application of solar updraft devices based on Trombe wall and beyond (e.g. double skin façade, ventilation solar chimney) for wider and different applications (e.g. greenhouse gas removal).

In this work, we have conducted both experimental measurements and numerical modelling. We mainly focus on investigating whether this type of devices can generate enough airflow under low solar conditions, and then developed a fast-analytical mathematical model to effectively and efficiently find design rules for further applications. One of the possible applications is to install them on dairy farms, stand alone or integrated with livestock buildings, where large amount of GHGs are emitted (e.g. CO_2, CH_4, etc.)

2. Methods

2.1 Experimental Setup

The experimental testing system was set up to investigate the performances of air heating and air flow rate in a simplified solar updraft device. As shown in Fig. 2, the experimental set-up consists of 2 parts

(the solar updraft device and the measurement system). The experiment was conducted between July and October 2021, in an outdoor open area at the King's Building campus of the University of Edinburgh, Edinburgh (55.9533° N, 3.1883° W), UK. The testing parameters, including the airflow velocity, inlet and outlet air temperature, ambient temperature, wind velocity and solar radiation intensity, all measured by in-situ sensors and a weather station as indicated in Fig 2. Real time monitoring data is collected and analyzed by the computer.

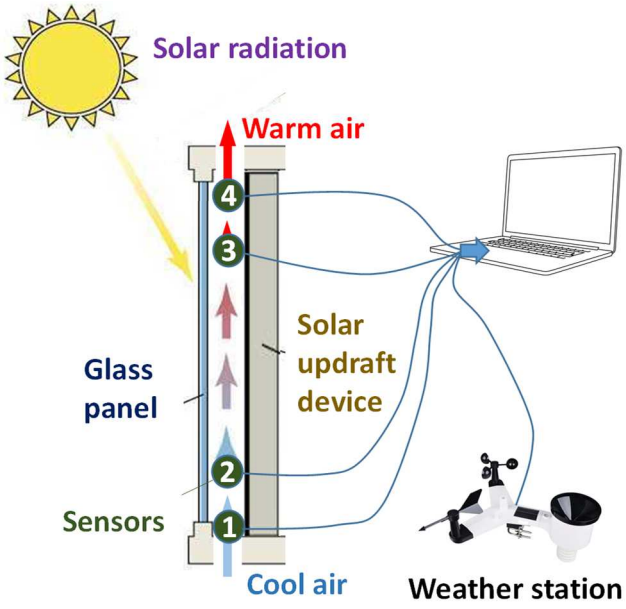

Fig. 2. Schematic diagram of the experimental testing system.

2.2 Mathematical modelling

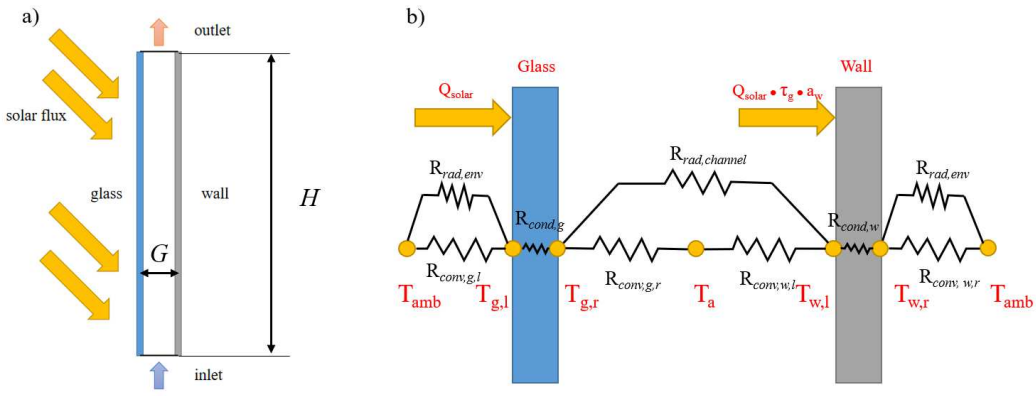

Fig. 3. a) 2D geometry (H is the height of the glass and the absorber, G denotes the wall-glass spacing); b) Thermal resistance network describing the flow of thermal energy inside the simplified solar updraft device.

The geometrical parameters of a simplified solar updraft device are shown in Fig. 3a, where *H* is the height of the glass and the absorber, *G* denotes the wall-glass spacing. As shown in Fig. 3b, the thermal resistance network illustrates the heat transfer process of the thermal behavior of the system. The main driving force of the flow inside a simplified solar updraft device is solar radiation, similar to other passive solar systems. An overall energy balance on the channel is considered. Certainly, there is some error caused by the approximated solution, since some assumptions are made to enable solving the mathematical model. The following assumption was made for modelling:

1. The Flow through the entire system was under steady-state conditions.

2. One-dimensional heat transfer was considered for all energy transfer processes through the absorber plate, glass and air channel.

3. Temperature at different points along the y direction on the glass and absorber were treated to be equal.

4. Temperature of inlet air was assumed to remain unchanged during calculation.

5. Airflow in the channel was considered as non-radiation absorbing fluid.

6. All thermal physical properties and wind velocity were evaluated at an average temperature.

In order to simulate our system under conditions close to reality, it is essential to choose material properties that represent the experimental system. The materials used in our model were shown in Table 1.

Table 1. Detail parameters of a simplified solar updraft device for calculation [17].

Type	Parameters	Symbols	Values	Units
Glass	Absorptivity	α_g	0.1	-
	Transmittance	τ_{g1}	0.75	-
	External Emissivity	ε_{ex}	0.9	-
	Internal Emissivity	ε_{in}	0.3	-
	Density	ρ	2220	kg/m^3
	Heat Capacity	C_p	800	J/(kg.K）
	Thermal Conductivity	k	1.38	W/(m·K)
	Glass thickness	d_g	0.005	m
	Glass length	L_g	0.5	m
	Glass height	H_g	1.8	m

Absorbing Wall	Absorptivity	a_w	0.9	-
	Transmittance	τ_{g2}	0.91	-
	External Emissivity	ε_{ex}	0.9	-
	Internal Emissivity	ε_{in}	0.3	-
	Density	ρ	1200	kg/m^3
	Heat Capacity	C_p	1250	J/(kg.K）
	Thermal Conductivity	k	0.3	W/(m·K)
	Wall thickness	d_w	0.2	m
	Wall length	L_w	0.5	m
	Wall height	H_w	1.8	m
Air	Density	ρ	1.18	kg/m^3
	Heat Capacity	C_a	1100	J/(kg.K）
	Thermal conductivity	k	0.026	W/(m·K)
	Kinematic viscosity	v_a	1.27e-5	m^2/s
	Thermal diffusivity	β	22.39e-6	m^2/s
	Dynamic viscosity	η	1.802e-5	kg m^{-1} s^{-1}
	Air inlet area	A_{in}	0.06	m^2
	Air outlet area	A_{out}	0.06	m^2
	Air channel gap	d_a	0.12	m
	The ratio of A_{out} / A_{in}	A_r	1	-

2.2.1 Energy balance over the flowing air

Energy balance equation for the air between glass cover and absorber can be expressed as

[Convection from absorber] + [Convection from glass] = [useful heat gain by the air]

It can mathematically be written as

$$\gamma_m \dot{m} c_p (T_i - \bar{T}_a) + h_{w,l} A_w (T_{w,l} - \bar{T}_a) + h_{g,r} A_g (T_{g,r} - \bar{T}_a) = 0 \qquad (1)$$

Where r_m is mass flow rate modification factor, 3.2.

An average temperature for the air flowing through the channel can be computed using a weighting factor between the inlet and outlet temperature as

$$\bar{T}_a = \omega T_o + (1 - \omega) T_i \qquad (2)$$

Where w (mean temperature weighting factor) is 0.4 [27].

So the above equation can be rewritten as

$$a_2 T_{w,l} + a_3 T_{g,r} - (a_1 + a_2 + a_3)\bar{T}_a = -a_1 T_i \quad (3)$$

Where $a_1 = \gamma_m \dot{m} c_p,\ a_2 = h_{w,l} A_w,\ a_3 = h_{g,r} A_g.$

2.2.2 Energy balance over the glass

The energy balance equation for the glass cover can be expressed as

[Incident solar radiation] + [radiation heat gain by glass cover from absorber] = [convective heat loss to air in flow channel] + [overall heat loss coefficient from glass to ambient]

It can mathematically be written as

$$S_{in} a_g A_g + hr_{w-g} A_w (T_{w,l} - T_{g,r}) + h_g A_g (\bar{T}_a - T_{g,r}) + U_t A_g (T_{amb} - T_{g,r}) = 0 \quad (4)$$

Where U_t stands for three heat transfer coefficients as

$$U_t = \frac{1}{1/h_{wind} + 1/h_{r,g-sky}} + h_{g,cond} \quad (5)$$

So the above equation can be rearranged as

$$b_2 T_{w,l} + b_3 \bar{T}_a - (b_2 + b_3 + b_4) T_{g,r} = -(b_1 + b_4 T_{amb}) \quad (6)$$

Where $b_1 = S_{in} a_g A_g,\quad b_2 = hr_{w-g} A_w,\quad b_3 = h_{g,r} A_g,\quad b_4 = U_t A_g.$

2.2.3 Energy balance over the absorber

The energy balance equation for the wall can be expressed as

[Solar radiation] = [convection to air in flow channel] + [long wave re-radiation to glass] + [conduction to the surroundings]

It can mathematically be written as

$$S_{in} \tau_g a_w A_w + hr_{w-g} A_w (T_{g,r} - T_{w,l}) + h_w A_w (\bar{T}_a - T_{w,l}) + U_b A_w (T_{amb} - T_{w,l}) = 0 \quad (7)$$

Rearranging the above equation gives

$$-(c_2 + c_3 + c_4) T_{w,l} + c_2 T_{g,r} + c_3 \bar{T}_a = -(c_1 + c_4 T_{amb}) \quad (8)$$

Where $c_1 = S_{in}\tau_g a_w A_w,\ c_2 = hr_{w-g}A_w,\ c_4 = U_b A_w$.

Where U_b stands for the overall heat transfer coefficient from the absorber wall to the surrounding, and it is calculated as:

$$U_b = \frac{1}{1/h_{wr} + d_w/k_w}$$

Where k_w stands for thermal conductivity of wall; h_{wr} stands for convective heat transfer coefficient between vertical absorber wall and the surrounding [=8 W m^{-2} K^{-1}]; d_w stands for wall thickness.

The above three equations (3), (6) and (8) can be iteratively solved using the relaxation method. So the temperature of the air in between, glass and absorber are gained. And the flowing air properties are treated to change with its temperature. The properties are renewed with the converged temperature values.

2.2.4 Mean temperature matrix

Generally, the above equations (3), (6) and (8) can be written in a 3x3 matrix form:

$$\begin{bmatrix} a_2 & a_3 & -(a_1+a_2+a_3) \\ b_2 & -(b_2+b_3+b_4) & b_3 \\ -(c_2+c_3+c_4) & c_2 & c_3 \end{bmatrix} \begin{bmatrix} T_{wl} \\ T_{gr} \\ T_a \end{bmatrix} = \begin{bmatrix} -a_1 T_i \\ -(b_1 + b_4 T_{amb}) \\ -(c_1 + c_4 T_{amb}) \end{bmatrix} \quad (9)$$

The matrix can be expressed as

$[A]\,[T] = [B]$ (10)

The mean temperature vector can be solved by matrix inversion:

$[T] = [A]^{-1}[B]$ (11)

A computer program was developed by MATLAB®, following the 5 main procedures shown in Fig.8. This procedure includes the following steps:

1. In the Input Process, all physical properties and design parameters of the simplified solar updraft device in Table 1 were input. The total time period was set as 24 hours for this simulation. Weather data (including ambient Temperature, solar radiation intensity) from experiments were input. The initially estimated temperature (T_a, T_{gr}, T_{wl}) of air, glass and massive wall were input.

2. In the Setting Process, T_{wl}, T_{gr} and T_a from the previous time step were used to estimate Ra and Pr by equations in Table 4. And then Ra and Pr were used to calculate Nu_g and Nu_w. hr_{mg}, U_b, h_{wr}, $hr_{g,sky}$, U_t, mass flow rate, air physical properties were attained from equations in Table 3.

3. In the Solving Process, all the required variables were subsequently put into a 3x3 matrix and the associated equations were solved by using an iterative process until the solution converged in the MATLAB program.

4. In the Time Control Process, the above procedures were repeated until the total running time reaches the total simulation time period.

5. The overall data were exported and graphed.

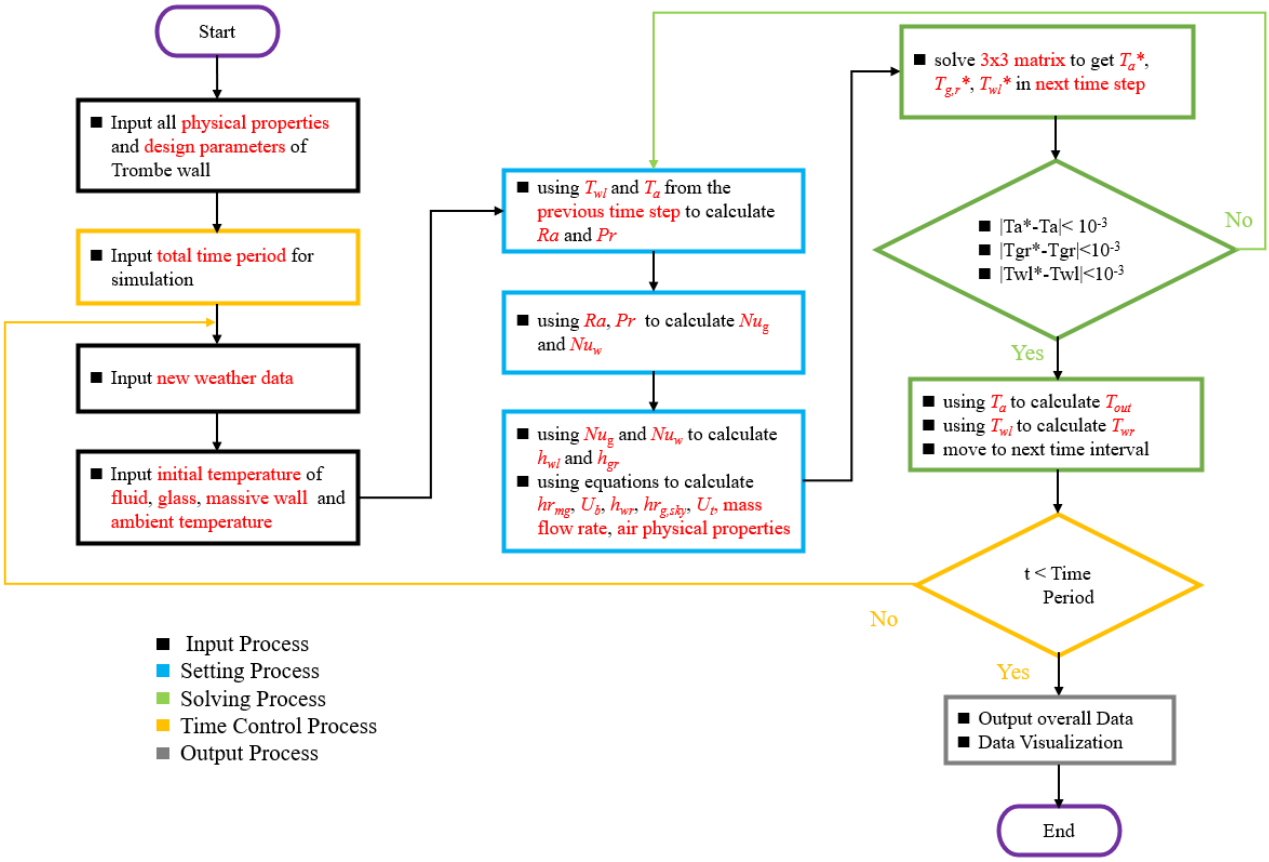

Fig. 4. Flow chart of the iterative procedures to solve the governing equations in MATLAB®.

2.2.5 Equations for physical properties

Equations applied for calculating heat transfer coefficients and the air physical properties are given in Table 2 and 3.

Table 2. Equations for heat transfer coefficient [27].

No.	Symbol	Description	Equations
1	h_{wind}	The convective heat transfer coefficient from wind	$h_{wind} = 5.7 + 3.8V$ where V is wind velocity [m s^{-1}].
2	T_{sky}	Sky temperature	$T_{sky} = 0.0552T_{amb}^{1.5}$ where T_{amb} and T_{sky} units are K.
3	$hr_{w\text{-}g}$	The radiative heat transfer coefficient between the massive wall and the glass	$hr_{m-g} = \sigma \frac{(T_{g,r}^2 + T_{w,l}^2)(T_{g,r} + T_{w,l})}{1/\varepsilon_g + 1/\varepsilon_w - 1}$ where $T_{g,r}$ and $T_{w,l}$ units are K.
4	$hr_{sky\text{-}g}$	The radiative heat transfer coefficient from the outer glass surface to the sky	$hr_{g-sky} = \frac{\sigma\varepsilon_g(T_{g,l} + T_{sky})(T_{g,l}^2 + T_{sky}^2)(T_{g,l} - T_{sky})}{(T_{g,l} - T_a)}$ where $T_{g,l}$ and T_{sky} units are K.
5	$h_{g,r}$	The convective heat transfer coefficient between glass and air in the flow channel	$h_{g,r} = \frac{NuK_f}{L_g}$ where L is the height of glass [m]; K_f is the air thermal conductivity [W m^{-1} K^{-1}]
6	$h_{w,l}$	The convective heat transfer coefficient between wall and air in the flow channel	$h_{w,l} = \frac{NuK_f}{L_w}$ where L is the height of absorber wall [m]; K_f is the air thermal conductivity [W m^{-1} K^{-1}]

Table 3. Equations for air physical properties [28].

No.	Description	Glass surface and air	Absorber wall and air
1	Mean temperature	$T_m = (T_{g,r} + T_a)/2$	$T_{m1} = (T_{w,l} + T_a)/2$
2	Coefficient of volumetric expansion	$\beta = 1/T_m$	$\beta_1 = 1/T_m$
3	Temperature difference	$\Delta T = T_{g,r} - T_a$	$\Delta T_1 = T_{w,l} - T_a$
4	Dynamic viscosity of air	$\mu_f = [1.846 + 0.00472(T_m - 300)]$	$\mu_{f1} = [1.846 + 0.00472(T_{m1} - 300)]$
5	Density of air	$\rho_f = [1.1614 - 0.00353(T_m - 300)]$	$\rho_{f1} = [1.1614 - 0.00353(T_{m1} - 300)]$
6	Thermal conductivity of air	$k_f = [0.0263 + 0.000074(T_m - 300)]$	$k_{f1} = [0.0263 + 0.000074(T_{m1} - 300)]$
7	Specific heat of air	$C_f = [1.007 + 0.00004(T_m - 300)] \times 10^3$	$C_{f1} = [1.007 + 0.00004(T_{m1} - 300)] \times 10^3$
8	Prandtl number	$Pr = \mu_f C_f / k_f$	$Pr = \mu_{f1} C_{f1} / k_{f1}$
9	Kinematic viscosity of air	$v_f = \mu_f / \rho_f$	$v_{f1} = \mu_{f1} / \rho_{f1}$
10	Grashof number	$Gr = g\beta\Delta T L_s^3 / v^2$	$Gr_1 = g\beta_1 \Delta T_1 L_s^3 / v^2$
11	Rayleigh number	$Ra = GrPr$	$Ra_1 = Gr_1 Pr_1$
12	Nusselt number (Laminar flow)	$Nu = 0.68 + (0.67Ra^{1/4})(1 + (0.492/Pr)^{9/16})^{4/9}$	$Nu_1 = 0.68 + (0.67{Ra_1}^{1/4})(1 + (0.492/Pr_1)^{9/16})^{4/9}$
13	Nusselt number (turbulent flow)	$Nu = \{0.825 + (0.38Ra^{1/6})(1 + (0.492/Pr)^{9/16})^{8/27}\}^2$	$Nu_1 = \{0.825 + (0.38{Ra_1}^{1/6})(1 + (0.492/Pr_1)^{9/16})^{8/27}\}^2$
14	Mass flow rate	$m = C_d \frac{\rho_f A_o}{\sqrt{1+A_r}} \sqrt{\frac{2gL_g(T_a - T_{amb})}{T_{amb}}}$ where L is height of glass or wall [m]; Value of the coefficient of discharge 'C_d' is taken as 0.396.	$m_1 = C_d \frac{\rho_{f1} A_o}{\sqrt{1+A_r}} \sqrt{\frac{2gL_w(T_a - T_{amb})}{T_{amb}}}$ where L is height of glass or wall [m]; Value of the coefficient of discharge 'C_d' is taken as 0.396.
15	Mean air velocity	$V_a = \frac{m}{\rho_f A_o}$	$V_{a1} = \frac{m_1}{\rho_{f1} A_o}$

2.3 Numerical analysis

2.3.1 Physical model and governing equations

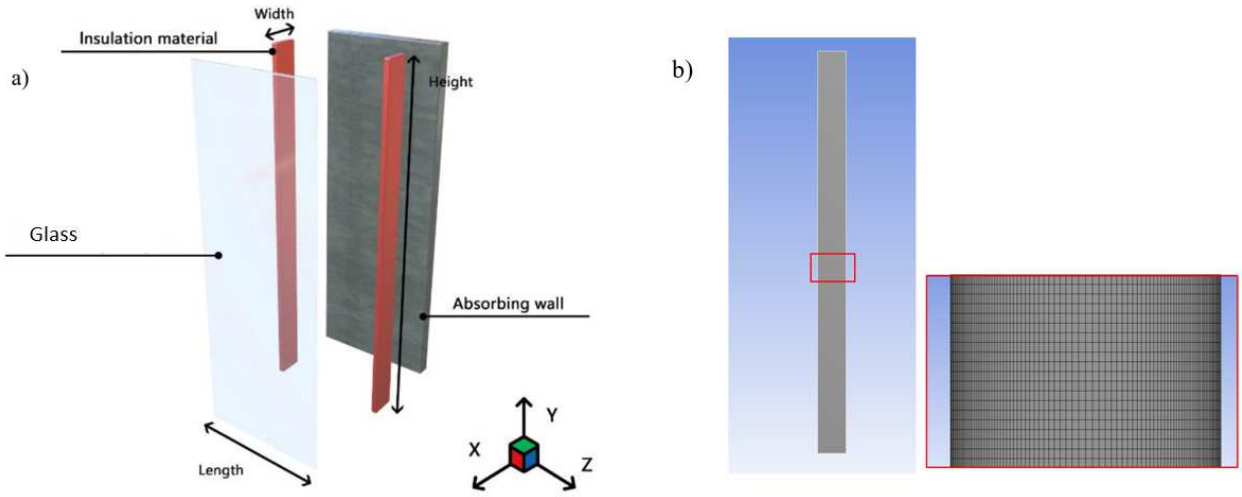

Fig. 5. a) 3D geometry; b) Mesh structure of the simplified solar updraft device.

The thermophysical characteristics of the fluid are constant, with the exception of the density change of the buoyancy term in the momentum equation along vertical direction, for which the Boussinesq approximation is utilized.

$$(\rho - \rho_0)g \cong -\rho_0 \beta (T - T_0)g \qquad (12)$$

In addition, the subsequent presumptions are made. Every surface is seen as a gray and diffuse surface, with the absorbing wall's and the horizontal wall's backsides being regarded as insulated. The temperature variations in the glass cover and absorbent wall's thickness directions are disregarded.

A 2D model is built to analyze the simplified solar updraft device. ANSYS Fluent (2019 R1) can solve the Navier-Stokes equations, and the main governing equations are expressed as follows [29]:

Continuity equation,

$$\frac{\partial \rho}{\partial t} + \frac{\partial (\rho u_i)}{\partial x_i} = 0 \qquad (13)$$

Where *t* is time, ρ is the density and u_i is the velocity vector of the fluid.

Momentum equation,

$$\frac{\partial(\rho u_i)}{\partial t}+\frac{\partial(\rho u_i u_j)}{\partial x_i}=-\frac{\partial P}{\partial x_i}+\frac{\partial}{\partial x_i}\left[(\mu+\mu_t)\left(\frac{\partial u_i}{\partial x_j}+\frac{\partial u_j}{\partial x_i}\right)-\frac{2}{3}\rho k\delta_{ij}\right]-\rho g\beta(T-T_0) \quad (14)$$

Where *P* is the pressure, Pa; u_i and u_j are components of velocity in various directions, m/s; x_i and x_j are coordinate components, m;

Energy equation,

$$\frac{\partial(\rho \mathrm{T})}{\partial t}+\frac{\partial(\rho u_i \mathrm{T})}{\partial x_i}=\mu_i\frac{\partial P}{\partial x_i}+\frac{\partial}{\partial x_i}\left(\frac{\lambda}{C_P}\frac{\partial T}{\partial x_i}+\frac{\mu_t}{\sigma_T}\frac{\partial T}{\partial x_i}\right) \quad (15)$$

Where C_P is specific heat, J/(kg K); σ_T is turbulent Prandtl number.

Turbulence kinetic energy *k* equation:

$$\frac{\partial(\rho \mathrm{k})}{\partial t}+\frac{\partial(\rho k u_i)}{\partial x_i}=\frac{\partial}{\partial x_i}\left[(\mu+\frac{\mu_t}{\sigma_k})\frac{\partial k}{\partial x_i}\right]+G_k+G_b-\rho\varepsilon-2\mu\left(\frac{\partial k^{\frac{1}{2}}}{\partial \mathrm{n}}\right)^2 \quad (16)$$

Specific rate of dissipation ε equation:

$$\frac{\partial(\rho\varepsilon)}{\partial t}+\frac{\partial(\rho u_i\varepsilon)}{\partial x_i}=\frac{\partial}{\partial x_i}\left[(\mu+\frac{\mu_t}{\sigma_\varepsilon})\frac{\partial \varepsilon}{\partial x_i}\right]+f_1 C_{1\varepsilon}\frac{\varepsilon}{\mathrm{k}}(G_k+C_{3\varepsilon}G_b)-f_1 C_{2\varepsilon}\rho\frac{\varepsilon^2}{\mathrm{k}}+2\frac{\mu\mu_t}{\rho}\left(\frac{\partial^2\mu}{\partial \mathrm{n}^2}\right)^2 \quad (17)$$

μ_t, a measure of the turbulent viscosity of a fluid:

$$\mu_t=C_\mu f_\mu \rho\frac{k^2}{\varepsilon} \quad (18)$$

$$f_\mu=exp\left(\frac{-2.5}{1+\rho\frac{k^2}{50\varepsilon\mu}}\right) \quad (19)$$

$$f_2=1-0.3exp\left(-\frac{\rho^2k^2}{\varepsilon^2\mu^2}\right) \quad (20)$$

$$G_k=\mu_t\left(\frac{\partial u_i}{\partial x_j}+\frac{\partial u_j}{\partial x_i}\right)\frac{\partial u_i}{\partial x_j} \quad (21)$$

$$G_b=-g\beta\frac{\mu_t}{\sigma_T}\frac{\partial T}{\partial x_j} \quad (22)$$

Where the Prandtl number of turbulent energy is given by σ_k, the rate of dissipation is given by ε, and the wall's normal coordinate is given by n; f_1 , f_2 and f_μ are the correction factors, and $C_{1\varepsilon}$, $C_{2\varepsilon}$, $C_{3\varepsilon}$ and C_μ are empirical constants. G_k and G_b are the generation term of the turbulent kinetic energy k due to the average velocity gradient and the generation term for the kinetic energy k caused by buoyancy, respectively.

2.3.2 Boundary conditions

According to the assumption, the temperature of the glass and wall are time-dependent, controlled by the UDF profile. Previous studies show that the temperature of the glass and wall is proportional to radiation intensity, which can be expressed as follow:

$$T_{wall} \propto I_{rad} \quad (23)$$

$$T_{glass} \propto I_{rad} \quad (24)$$

Wu et al. studies show that channel height and channel width mainly affect the temperature of the glass and wall [13, 14]. So all the temperatures can be expressed as follows:

$$T_{wall} \propto f(H, W) \quad (25)$$

$$T_{glass} \propto f(H, W) \quad (26)$$

Combined from (23)-(26), T_{glass} and T_{wall} can be expressed as follows:

$$T_{wall} = T_{amb} + t\sigma_{wall} I_1 \, sin(0.5\pi I_{rad}/I_0) \, e^{0.7\, cos(0.25\pi H/H_0)} (W/W_0)^{\beta} \quad (27)$$

$$T_{glass} = T_{amb} + t\sigma_{glass} I_1 \sin(0.5\pi I_{rad}/I_0) e^{0.7\, cos(0.25\pi H/H_0)} (W/W_0)^{\beta} \quad (28)$$

Where T_{amb} is the ambient temperature, K; t is flow time, s; σ_{wall} and σ_{glass} stand for the heat transfer modification factors of wall and glass, which are 12e-5 and 8.0e-5 respectively. I_1 stands for the solar radiation intensity modification factor, which is 200 W/m^2; I_0 stands for the standard solar radiation intensity, which is 1000W/m^2. I_{rad} stands for the current solar radiation intensity, W/m^2. W_0 and H_0 stand for the standard length of width and height, m, which are 0.14 and 1.8 m, respectively. β stands for the width modification factor, which is -0.8.

Table 4. All parameters for boundary conditions

Boundary Type	Momentum	Values	Thermal	Values
Inlet	Velocity Specification Method	Magnitude, Normal to Boundary	Temperature (K)	UDF Temperature Profile
	Velocity Magnitude (m/s)	0.4		
	Turbulence Specification Method	Intensity and Viscosity Ratio		
	Turbulence Intensity (%)	5		
	Turbulence Viscosity Ratio	10		
Absorbing Wall	Wall Motion	stationary wall	Temperature (K)	UDF Temperature Profile
	Shear Condition	no slip		
	Roughness Models	standard		
Outlet	Backflow Direction Specification Method	Normal to Boundary	Temperature (K)	UDF Temperature Profile
	Backflow Pressure Specification	Total Pressure		
	Turbulence Specification Method	Intensity and Viscosity Ratio		
	Turbulence Intensity (%)	5		
	Turbulence Viscosity Ratio	10		
Glass	Wall Motion	stationary wall	Temperature (K)	UDF Temperature Profile
	Shear Condition	no slip		
	Roughness Models	standard		

2.3.3 Fluent Models and Solvers

The transient state results are provided to reflect the ultimate performance of the novel Trombe wall. The chosen time step size is 30 s, and there are 120 total time steps. Table 5 and 6 show the main setting, parameters and the corresponding values used in the calculation.

Table 5. Basic setting applied in CFD model

Setting	Model	Reason
Density	Boussinesq approximation	To consider buoyancy effect
Energy	Activated	To consider heat transfer
Radiation	UDF	To consider solar radiation
Turbulence	Standard k-epsilon Model	To consider turbulence effect

Table 6. Numerical solution methods chosen

Application zone	Methods
Pressure-Velocity Coupling	SIMPLE
Spatial discretization	Least Squares Cell Based
Pressure	Second Order
Momentum	Second Order Upwind
Turbulent Kinetic Energy	First Order Upwind
Turbulent Dissipation Rate	First Order Upwind
Transient Formulation	First Order Implicit
Energy	Second Order Upwind

2.3.4 Mesh independence test

The computation domain in this study is shown in Fig. 5a. Under optimized conditions, the reactor's height is 1.8 m, which would be changed according to the research purpose. The reactor's width is 0.12m, which also would vary according to the research purpose. The gas does not take part in the radiative heat transfer, and the thermophysical properties of fluid almost remain constant, but air density does change because of the buoyancy term in the momentum equation along the vertical direction, which the Boussinesq approximation is used. As shown in Fig. 5b, mesh refinement was applied in the boundary layer region and was adopted to prove a grid-independent solution. When the mesh number exceeds 5000, the greatest discrepancy between V_{out} and T_{out} is less than 1%, according to the findings of the mesh independence test. By comparison, 40,000 quadrilateral meshes are proven

to be sufficient to meet the mesh independent verification criterion.

3. Results and discussions

3.1 Experimental setup and data

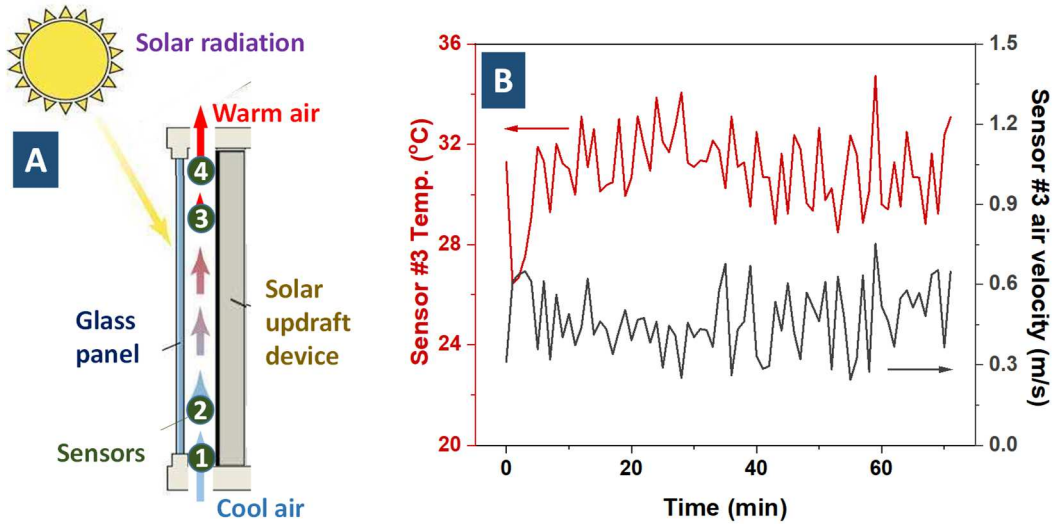

Fig. 2 A) Illustration of the test rig, which is adapted from a solar updraft Trombe wall, 1.8 m high × 0.5 m wide × 0.12 m thick). B) Temp. rise and velocity of airflow measured in the rig under 397 W/m^2 solar radiation.

A test rig was built outdoor according to the illustrated design in Fig. 2A, which is adapted from a solar updraft Trombe wall. Instead of a "C"-shaped flow channel with an inlet and outlet perpendicular to the vertical air flow direction, this rig simplified the design and only included the main vertical channel with inlet and outlet aligned directly at both ends. This simplified model could provide generality for other formats of solar updraft designs, for example, double skin façade and ventilation solar chimney. The size of the airflow channel is 1.8 m height × 0.5 m width × 0.12 m air cavity thickness (i.e. the gap between the glass panel and the wall is 0.12 m), which is decided based on the best flexibility to be field tested on dairy farms. Four sensors were fitted in the airflow channel to measure airflow temperature and velocity. Experimental data were collected on different days under various solar radiation conditions. Fig. 2B shows the typical air temperature rise (6.4 ºC) and airflow velocity (0.46 m/s) in the airflow channel on a particular day with solar radiation of 397 W/m^2 at the time of the measurement.

More data measured under a wide range of solar radiation (from 100 W/m^2 to 600 W/m^2) is summarised and presented in Figures 3 and 4. It can be clearly seen that when the solar radiation is low (i.e. 100 W/m^2), the air temperature rise (1.6 ºC), airflow velocity (0.13 m/s) and mass flowrate (33.1 kg/hr) in the airflow channel are low, too. When solar radiation grows, the air temperature rise and airflow velocity increase, due to receiving more solar energy. The most exciting observation is that there is a rapid increase in air temperature rise and airflow velocity once the solar radiation moves above 100 W/m^2. At solar radiation of 120 W/m^2, air temperature rise, airflow velocity and mass flowrate increase significantly to 4.4 ºC, 0.31 m/s and 75.6 kg/hr, respectively. When solar radiation grows further, the air temperature rise, airflow velocity and mass flowrate increase slowly towards 6.5 ºC, 0.45m/s and 115 kg/hr, respectively.

Therefore, the experimental results prove that the air mass flowrate generated by solar updraft in a 0.9 m^2 solar updraft device can be as high as 75.6 kg/hr when the solar radiation is only 120 W/m^2, which is not a high threshold (achievable on 281 days, or 1600 hours, in 2020 in south England [30]).

3.2 Model validation

Research in the field reveals that different dimension of a Trombe wall has a great impact on the solar updraft (i.e. temperature rise, airflow velocity and mass flowrate). Numerical modelling is an effective and efficient way to find more insights, which can provide guidance for design and future applications.

Ansys Fluent is a commercially available option for CFD modelling. We also tried to develop a mathematical model based on more widely available MATLB and expected it to be more efficient as it needs less computing resources.

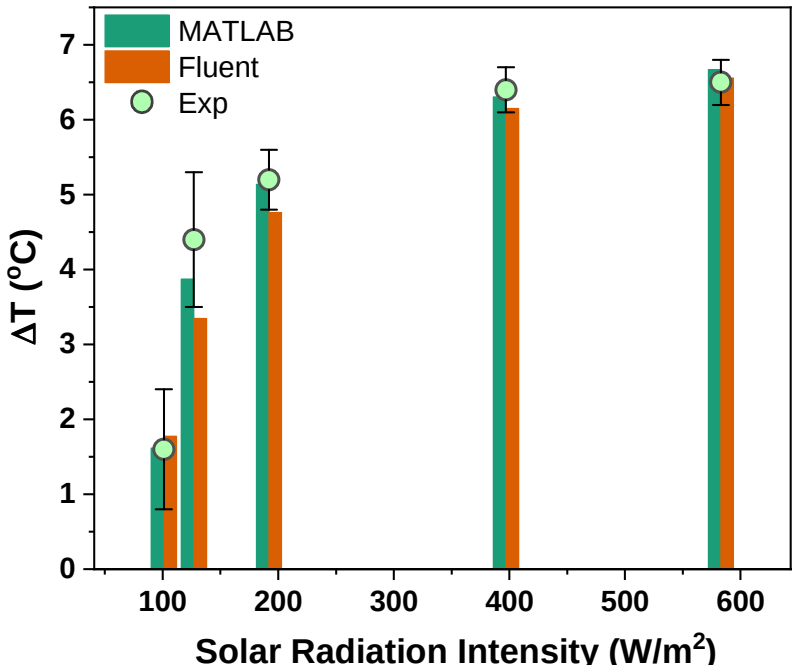

Fig.3. Comparison of ΔT (air temp. difference of inlet and outlet) under different solar intensity.

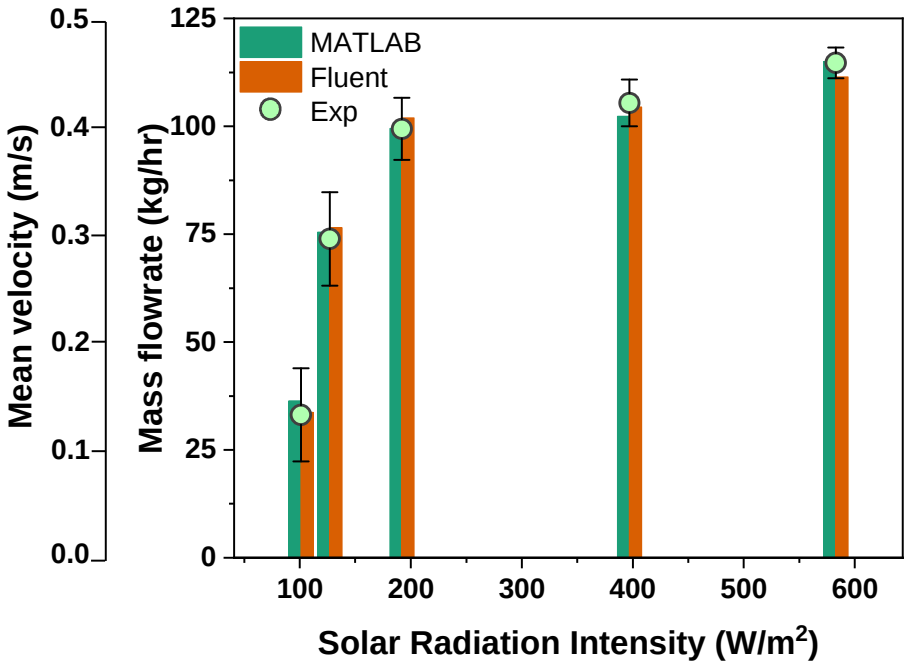

Fig. 4. Variations of Mass flow rate under different solar intensity.

To validate the accuracy of the two models, they were validated by comparing with the data from the experiment as shown in Fig. 3 and 4. The *RSMD* (root mean square deviation) is considered as an evaluation indicator to analyze the error between the simulation and experiment. The *RSMD* is calculated using the following expression:

$$RSMD = \sqrt{\frac{\sum\left[\left(X_{ref} - X_{sim}\right)/X_{ref}\right]^2}{n}} \times 100\%$$

As shown in Fig. 3 and 4, it can be seen that the numerical results from both models have the same trend with the experimental values as the intensity of sunlight changes. The values of RSMD of air temperature difference and air mass flow rate from the MATLAB model are 5.03% and 4.48% respectively, while the values of those from the Fluent model are 8.56% and 2.52% respectively. It could be concluded that the numerical results have an acceptable agreement with the experimental data. Therefore, both models are reliable and can be confidently applied for further study of the performance of solar updraft devices.

Table 7. Comparison of MATLAB and Fluent models.

	MATLAB	Fluent
CPU Time	1.67 sec	353.65 sec
Memory Usage	217.09 KB	0.18 GB
Accuracy	4.76%	5.54%

Table 7 gives the comparison of the two models in more detail. It shows that the MATLAB model has the following advantages compared to the Fluent model: (1) get results faster; (2) take up less memory space; (3) the accuracy is also slightly higher; and also (4) it is more flexible, and all contents can be modified to suit specific needs. Of course, Fluent also has the advantage of more comprehensive visualization of flow characteristics and can account for more complicated conditions, while the MATLAB model can be considered as a fast-analytical tool. We do not intend to use one approach to replace the other, or use these two models for head-to-head comparisons, but develop a complementary tool set instead.

3.3 Applications of the Models

With the reliable models developed, we can investigate 1) how device dimensions will affect the solar updraft performances using the MATLAB model as a fast-analytical tool, 2) how the air moves and distributes in the airflow channel using the visualizability of the Fluent model.

Fig. 5 provides a comprehensive data set to show how device dimensions affect solar updraft

performances. In Fig 5a, when the air channel gap increases, ΔT decreases because of the increase of heat transfer distance and heat loss. As the height increases, ΔT increases. This is because the area of the device increases and it receives more solar flux, resulting in larger ΔT. From Fig. 5b, it can be seen that the trend of gap and height *vs.* airflow velocity is very similar to the thickness and height *vs.* ΔT. This is because ΔT is positively correlated to the buoyancy of air and thus airflow velocity.

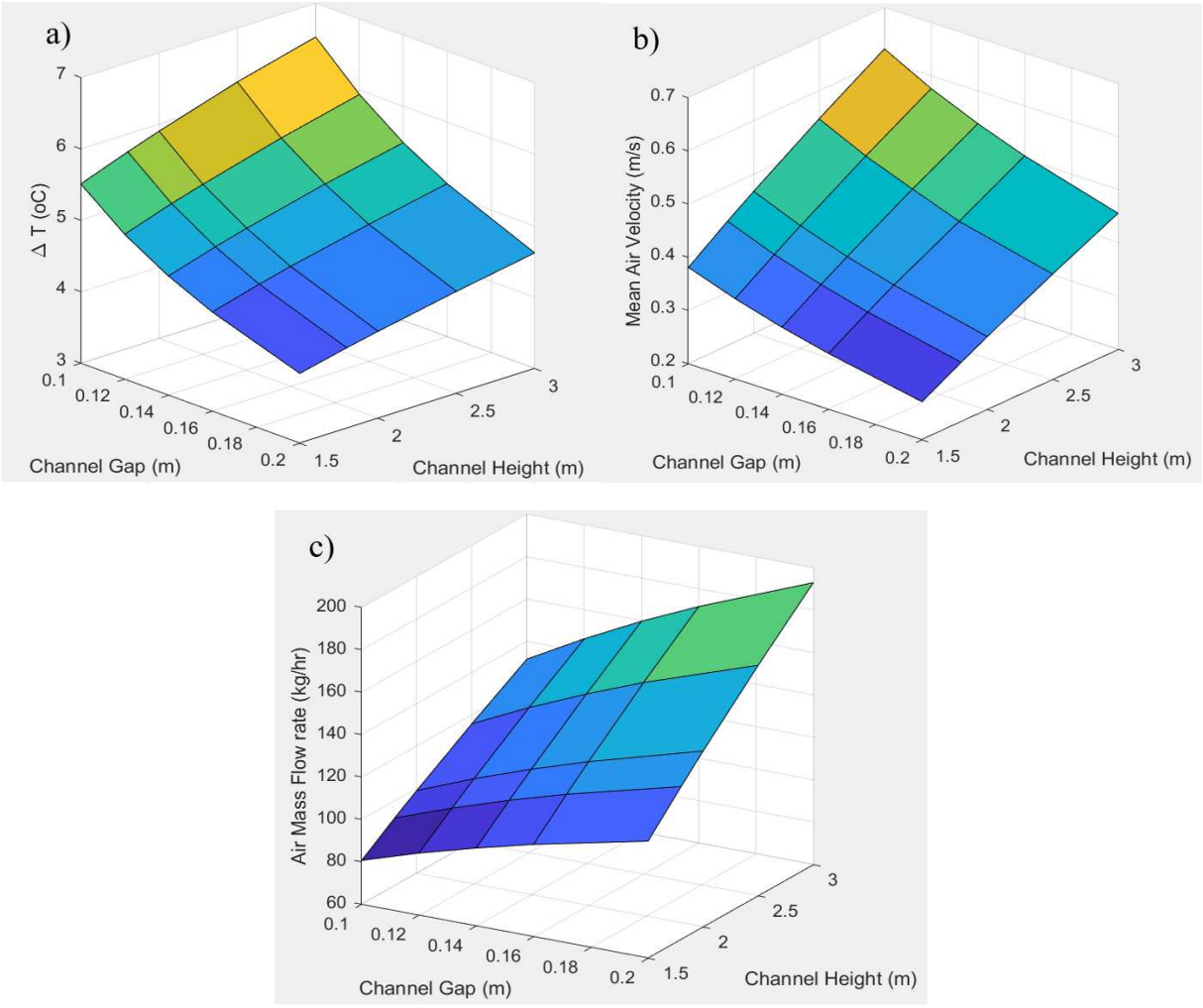

Fig. 5. Variations of a) ΔT *(*air temperature difference between inlet and outlet), b) Mean air velocity and c) Mass flow rate, with Channel Height and Channel Gap under 200 W/m^2 solar intensity.

Fig. 5c indicates how mass flowrate changes with gap and height. It is easy to understand that mass flowrate increases in the higher device because of higher airflow velocity. However, the influence of the air channel gap on mass flowrate is more complicated. When the channel gets thicker, mass flowrate increases although airflow velocity is slower. The reason is that thicker channel provides a larger cross-section area for the airflow.

The above observation can provide guidance for the design and applications of the device. For example, if high mass flowrate is the only target of an application, thicker and higher dimensions are preferable subject to available space and construction costs. If high airflow velocity and/or high air temperature is also needed for a particular application, there will be a compromise to decide on the optimum gap.

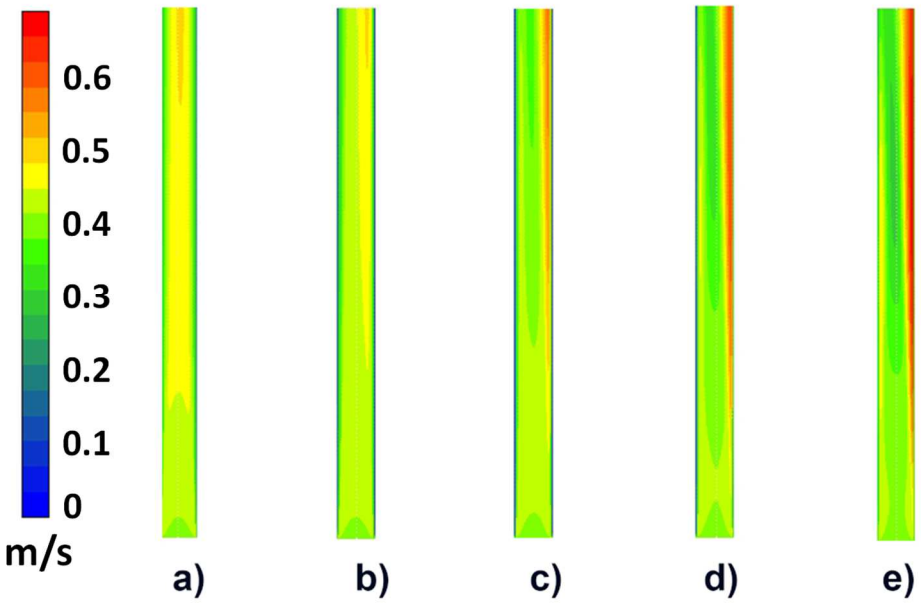

Fig. 6. The velocity contour under a) 100 W/m^2; b) 200 W/m^2; c) 400 W/m^2; d) 600 W/m^2; e) 800 W/m^2 solar intensity.

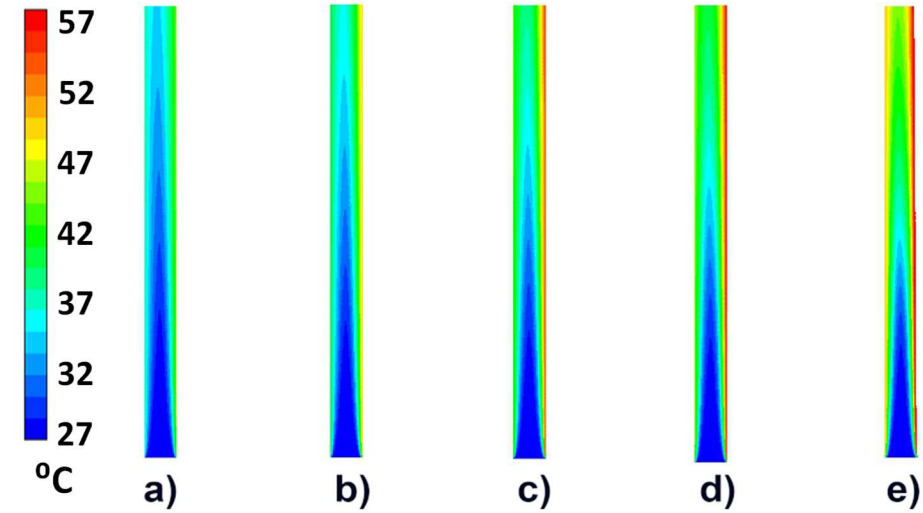

Fig. 7. Temperature Field under a) 100 W/m^2; b) 200 W/m^2; c) 400 W/m^2; d) 600 W/m^2; e) 800 W/m^2 solar intensity.

With the aid of Fluent model visualization, Figures 6 and 7 show how the air moves and distributes in the airflow channel. Fig. 6 reveals that, at low solar radiation, airflow close to both sides is slower than

that at the center and maximum airflow velocity exists at the center of the channel. When the solar radiation increases, the maximum airflow velocity will be distributed closer to the wall. Fig. 7 demonstrates that the highest air temperature always appears near the wall, while the air temperature in the center of the channel is the lowest.

When the device is later designed to facilitate CO_2 capture and drive photocatalytic decomposition of CH_4 and N_2O, if the materials or processes are sensitive to airflow velocity or air temperature, the above results can provide further guidance on where those materials are best fitted and how those processes are designed.

4. **Conclusion**

In this work, we have conducted both experimental measurements and numerical modelling to investigate whether a solar updraft device can generate enough airflow under low solar conditions, and then developed a fast-analytical mathematical model to effectively and efficiently find design rules for further application. We found that:

(1) The experimental results prove that the air mass flowrate generated by solar updraft in a 0.9 m^2 solar updraft device can be as high as 75.6 kg/hr when the solar radiation is only 120 W/m^2.

(2) Comparison of two numerical models shows that it is feasible to develop a fast-analytical tool based on widely available MATLAB with low demand of computing resources and to provide guidance on how a future device should be designed for particular applications.

Nomenclature

A_o， A_i	Cross-section areas of outlet and inlet to air flow channel [m^2]
A_r	the ratio of A_o/A_i
A_w， A_g	the surface area of the vertical wall and glass [m^2]
C_d	coefficient of discharge of air channel [=0.396]
C_f	specific heat of air [J kg^{-1} K^{-1}]
d	distance between wall and glass [m]
g	gravitational constant [= 9.81 m s^{-2}]
S_{in}	incident solar radiation on the vertical surface [W m^{-2}]
$h_{g,r}$	convective heat transfer coefficient between the right glass cover and air channel [W m^{-2} K^{-1}]
$h_{w,l}$	convective heat transfer coefficient between vertical left wall and air channel [W m^{-2} K^{-1}]
$hr_{g\text{-}sky}$	radiative heat transfer coefficient between glass cover and sky [W m^{-2} K^{-1}]
hr_{wg}	radiative heat transfer coefficient between vertical wall and glass cover [W m^{-2} K^{-1}]
h_{wind}	convective wind heat loss coefficient [W m^{-2} K^{-1}]
$h_{g,cond}$	The conductive heat transfer coefficients for glass [=9.41 W m^{-2} K^{-1}]
k_f	thermal conductivity of air [W m^{-2} K^{-1}]
k_w	thermal conductivity of wall [W m^{-2} K^{-1}]
H_w	height of wall [m]
m_a	mass flow rate [kg s^{-1}]
T_{amb}	ambient temperature [^oC]
T_a	mean temperature of the air in the channel [^oC]
T_i	the inlet temperature of the air in the channel [^oC]

T_o	The outlet temperature of the air in the channel [^{o}C]
$T_{g,r}$	right side glass cover temperature [^{o}C]
T_{sky}	sky temperature [K]
$T_{w,l}$	left side vertical wall temperature [^{o}C]
$T_{g,l}$	left side vertical glass temperature [^{o}C]
$T_{w,r}$	right side vertical wall temperature [^{o}C]
U_b	Overall convective heat transfer coefficient between the vertical wall and room [W m^{-2} K^{-1}]
U_t	Overall convective heat transfer coefficient from top of the glass cover [W m^{-2} K^{-1}]
V	wind velocity [= 2 m s^{-1}]
G	gap of air channel [m]
r_m	mass flow rate modification factor [=3.2]
w	mean air temperature weighting factor [=0.4]
a_g, a_w	Absorptivity of glass and wall
τ_g	Transmittance of glass

Dimensionless terms

Nu	Nusselts number
Pr	Prandtl number
Gr	Grashof number
Ra	Rayleigh number

Acknowledgement

We gratefully acknowledge the support by the European Commission H2020 Marie S Curie Research and Innovation Staff Exchange (RISE) award (Grant No. 871998), Department for Business, Energy and Industrial Strategy DAC and GGR Programme (Sch202036), and National Key Research and Development Plan (Key Special Project of Inter-governmental National Scientific and Technological Innovation Cooperation, Grant No. 2019YFE0197500).

Reference

[1] G. Realmonte, L. Drouet, A. Gambhir, J. Glynn, A. Hawkes, A.C. Köberle, M. Tavoni, An inter-model assessment of the role of direct air capture in deep mitigation pathways, Nat. Commun., 10 (1) (2019) 3277.

[2] F. Zeman, Energy and Material Balance of CO2 Capture from Ambient Air, Environmental Science & Technology, 41 (21) (2007) 7558-7563.

[3] R. de_Richter, T. Ming, P. Davies, W. Liu, S. Caillol, Removal of non-CO2 greenhouse gases by large-scale atmospheric solar photocatalysis, Prog. Energy Combust. Sci., 60 (2017) 68-96.

[4] R.K. de_Richter, T. Ming, S. Caillol, Fighting global warming by photocatalytic reduction of CO2 using giant photocatalytic reactors, Renew. Sust. Energ. Rev., 19 (2013) 82-106.

[5] Y. Huang, Y. Shao, Y. Bai, Q. Yuan, T. Ming, P. Davies, X. Lu, R. de Richter, W. Li, Feasibility of Solar Updraft Towers as Photocatalytic Reactors for Removal of Atmospheric Methane–The Role of Catalysts and Rate Limiting Steps, Front. Chem., 9 (2021).

[6] Ipcc, V. Masson-Delmotte, P. Zhai, H.-O. Pörtner, D. Roberts, J. Skea, P. Shukla, A. Pirani, W. Moufouma-Okia, C. Péan, R. Pidcock, S. Connors, R. Matthews, Y. Chen, X. Zhou, M. Gomis, E. Lonnoy, T. Maycock, M. Tignor, M. Tabatabaei, Global warming of 1.5°C. An IPCC Special Report on the impacts of global warming of 1.5°C above pre-industrial levels and related global greenhouse gas emission pathways, in the context of strengthening the global response to the threat of climate change, sustainable development, and efforts to eradicate poverty, 2018.

[7] M. Hulme, Intergovernmental Panel on Climate Change (IPCC), (2020) 1-7.

[8] D.A. Dowling, V. Ramakrishnan, Greenhouse gas removal report 2018, in, Royal Society Available online: https://royalsociety.org/-/media/policy/projects/greenhouse-gas-removal/royal-society-greenhouse-gas-removal-report-2018.pdf, 2018.

[9] D. Wang, L. Hu, H. Du, Y. Liu, J. Huang, Y. Xu, J. Liu, Classification, experimental assessment, modeling methods and evaluation metrics of Trombe walls, Renew. Sust. Energ. Rev., 124 (2020) 109772.

[10] O. Saadatian, K. Sopian, C.H. Lim, N. Asim, M.Y. Sulaiman, Trombe walls: A review of opportunities and challenges in research and development, Renew. Sust. Energ. Rev., 16 (8) (2012) 6340-6351.

[11] G. Gan, A parametric study of Trombe walls for passive cooling of buildings, Energy Build., 27 (1) (1998) 37-43.

[12] S. Lal, CFD simulation for the feasibility study of a modified solar chimney applied for building space heating, in, 2014.

[13] S.-Y. Wu, L. Xu, L. Xiao, Performance study of a novel multi-functional Trombe wall with air purification, photovoltaic, heating and ventilation, Energy Convers. Manage., 203 (2020) 112229.

[14] S.-Y. Wu, L. Xu, L. Xiao, Air purification and thermal performance of photocatalytic-Trombe wall based on multiple physical fields coupling, Renew. Energy, 148 (2020) 338-348.

[15] L. Du, L. Ping, C. Yongming, Study and analysis of air flow characteristics in Trombe wall, Renew. Energy, 162 (2020) 234-241.
[16] B. Yu, W. He, N. Li, L. Wang, J. Cai, H. Chen, J. Ji, G. Xu, Experimental and numerical performance analysis of a TC-Trombe wall, Appl. Energy, 206 (2017) 70-82.
[17] B. Yu, J. Hou, W. He, S. Liu, Z. Hu, J. Ji, H. Chen, G. Xu, Study on a high-performance photocatalytic-Trombe wall system for space heating and air purification, Appl. Energy, 226 (2018) 365-380.
[18] B. Yu, Q. Jiang, W. He, Z. Hu, H. Chen, J. Ji, G. Xu, The performance analysis of a novel TC-Trombe wall system in heating seasons, Energy Convers. Manage., 164 (2018) 242-261.
[19] B. Yu, J. Yang, W. He, M. Qin, X. Zhao, H. Chen, The performance analysis of a novel hybrid solar gradient utilization photocatalytic-thermal-catalytic-Trombe wall system, Energy, 174 (2019) 420-435.
[20] A. Mokni, A. Lashin, M. Ammar, H. Mhiri, Thermal analysis of a Trombe wall in various climatic conditions: An experimental study, Sol Energy, 243 (2022) 247-263.
[21] O.K. Ahmed, K.I. Hamada, A.M. Salih, Enhancement of the performance of Photovoltaic/Trombe wall system using the porous medium: Experimental and theoretical study, Energy, 171 (2019) 14-26.
[22] S.-Y. Wu, R.-R. Yan, L. Xiao, Numerically predicting the effect of fin on solar Trombe wall performance, Sustainable Energy Technologies and Assessments, 52 (2022) 102012.
[23] L. Zhang, J. Dong, S. Sun, Z. Chen, Numerical simulation and sensitivity analysis on an improved Trombe wall, Sustainable Energy Technologies and Assessments, 43 (2021) 100941.
[24] X. Hong, W. He, Z. Hu, C. Wang, J. Ji, Three-dimensional simulation on the thermal performance of a novel Trombe wall with venetian blind structure, Energy Build., 89 (2015) 32-38.
[25] H. Chen, S. Liu, M. Eftekhari, Y. Li, W. Ji, Y. Shen, Experimental studies on the energy performance of a novel wavy-shape Trombe wall, Journal of Building Engineering, 61 (2022) 105242.
[26] D. Burnett, E. Barbour, G.P. Harrison, The UK solar energy resource and the impact of climate change, Renew. Energy, 71 (2014) 333-343.
[27] K.S. Ong, A mathematical model of a solar chimney, Renew. Energy, 28 (7) (2003) 1047-1060.
[28] A. Abdeen, A.A. Serageldin, M.G.E. Ibrahim, A. El-Zafarany, S. Ookawara, R. Murata, Experimental, analytical, and numerical investigation into the feasibility of integrating a passive Trombe wall into a single room, Appl. Therm. Eng., 154 (2019) 751-768.
[29] ANSYS, ANSYS Fluent Tutorial Guide 18.0, in, ANSYS, Inc., Available online: http://www.pmt.usp.br/academic/martoran/notasmodelosgrad/ANSYS%20Fluent%20Tutorial%20Guide.pdf, 2017.
[30] Solcast.com, Historical solar irradiance data in south England, in, Retrieved from: https://solcast.com/, 2020.